Available online at www.sciencedirect.com
ScienceDirect
Computers and Geotechnics 35 (2008) 210–222
COMPUTERS AND GEOTECHNICS
www.elsevier.com/locate/compgeo

A unified constitutive model for both clay and sand with hardening parameter independent on stress path

Y.P. Yao [a,*], D.A. Sun [b], H. Matsuoka [c]

[a] Department of Civil Engineering, Beihang University, Beijing 100083, China
[b] Department of Civil Engineering, Shanghai University, Shanghai 200072, China
[c] Department of Civil Engineering, Nagoya Institute of Technology, Nagoya 466-8555, Japan

Received 31 August 2006; received in revised form 30 March 2007; accepted 30 March 2007
Available online 21 May 2007

Abstract

A unified constitutive model for both clay and sand under three-dimensional stress conditions is derived from the modified Cam-clay model, by taking the following two points into consideration. First, a transformed stress tensor based on the SMP (spatially mobilized plane) criterion is applied to the Cam-clay model. The proposed model consistently describes shear yielding and shear failure and combines critical state theory with the SMP criterion for clay. Secondly, a new hardening parameter, which is independent of the stress path, is derived in order to develop a unified constitutive model for both clay and sand. It not only describes the dilatancy for lightly to heavily dilatant sand, but also reduces to the plastic volumetric strain for clay. The validity of the hardening parameter is confirmed by the test results of triaxial compression and extension tests on sand under various stress paths. Only five conventional soil parameters are needed in the proposed model.

Keywords: Clay; Dilatancy; Elastoplastic model; Sand; Stress path; Three-dimensional stress

1. Introduction

The modified Cam-clay model, called the Cam-clay model for short in this paper, which is suitable for clay (in this paper, the term clay is to be interpreted as normally consolidated clay), was proposed by Roscoe and Burland [18]. The Cam-clay model and many other models have been generalized by assuming a section of the yield surface to be circular in the π-plane. The mean stress $p(=\sigma_{ii}/3)$ and deviator stress $q(=\sqrt{3/2}\sqrt{s_{ij}s_{ij}})$ are used as the stress parameters in the models, where $s_{ij}(=\sigma_{ij}-p\delta_{ij})$ is a deviatoric stress tensor and δ_{ij} is Kronecker's delta. That is to say, the criterion of the Extended Mises type ($\eta=q/p=$ const.) is adopted for the shear yielding and the shear failure of clay in the Cam-clay model. Shear yielding is caused by an increase in stress ratio $\eta=q/p$, while compressive yielding is caused by an increase in the mean stress p. However, as experimental evidence shows, the Extended Mises criterion grossly overestimates the strength in triaxial extension, and also results in incorrect intermediate stress ratios in plane strain [22]. In contrast to the Extended Mises failure, the SMP failure criterion [8], which is considered to be a three-dimensional extension of the Mohr–Coulomb criterion, is a failure criterion that explains the high quality test results for soils. A transformed stress tensor has been proposed by Matsuoka et al. [9] which makes the SMP criterion become circular in the transformed π-plane. A revised transformed stress tensor $\tilde{\sigma}_{ij}$ for the SMP criterion is developed in this paper based on the transformed stress method [9] and the work of Yao and Sun [24,25] in order to take the plastic strain increment direction into account additionally. The new transformed stress tensor $\tilde{\sigma}_{ij}$ is applied to the Cam-clay model. The proposed model consistently describes the shear yielding and shear failure of soils under three-dimensional stresses, both

* Corresponding author. Tel.: +86 10 82316111.
E-mail address: y-pyao@163.com (Y.P. Yao).

0266-352X/$ - see front matter © 2007 Elsevier Ltd. All rights reserved.
doi:10.1016/j.compgeo.2007.04.003

of which obey the SMP criterion, and combines critical state theory with the SMP criterion for clay.

Traditionally, the plastic volumetric strain ε_v^p is taken as the hardening parameter in the Cam-clay model, which is not appropriate for dilatant sand. To date, a lot of hardening parameters which can describe the dilatancy of soils have been assumed (e.g., [5,15,2,11,1,6]), and several dilatant plasticity models have been proposed (e.g., [4,16,17,27,3,26]). In this paper, a new hardening parameter, that is independent of stress path, is derived by considering unified yield and plastic potential functions which are the same those for Cam-clay. As will be described later, the physical meaning of this hardening parameter is clear. The proposed hardening parameter not only describes the dilatancy from lightly to heavily dilatant sand, but also reduces to the plastic volumetric strain ε_v^p for clay. The validity of the hardening parameter H is confirmed by triaxial compression and extension test results on sand under various stress paths.

The ability of the proposed model to predict the drained behavior of normally consolidated clay and saturated sand is examined along various stress paths under triaxial compression and extension conditions. The results predicted by the proposed model agree well with the test results. Only five soil parameters are needed in the proposed model. The values of these parameters can be determined by a loading and unloading isotropic compression test and a conventional triaxial compression test. In this paper, the term stress is to be interpreted as effective stress. The implementation of the model into the finite element method follows the methods described in Sheng et al. [20] and Sloan et al. [21].

2. A transformed stress tensor based on the SMP criterion

A transformed stress tensor, by which the SMP criterion is made circular in the transformed π-plane, has been proposed by Matsuoka et al. [9]. A revised transformed stress tensor $\tilde{\sigma}_{ij}$ is developed in this paper based on the transformed stress method [9] and the work of Yao and Sun [24,25] in order to take the plastic strain increment direction into account additionally. The outline of the new transformed stress tensor $\tilde{\sigma}_{ij}$ is introduced as follows:

The SMP criterion can be written as

$$I_1 I_2 / I_3 = \text{const} \tag{1}$$

where I_1, I_2 and I_3 are the first, second and third stress invariants, respectively. The solid curve in Fig. 1 is the shape of the SMP criterion in the π-plane. The transformed stress is deduced from what makes the SMP curve in the π-plane become a circle, the dot line of Fig. 1, with the center being the origin in the transformed π-plane ($\tilde{\pi}$-plane).

When $p = \text{const}$, we assume that $\tilde{r}$ is equal to r_0, where $\tilde{r}$ is the stress radius in the π-plane of the transformed stress space and r_0 is the stress radius in the π-plane of the ordinary stress space when $\theta = 0$. From Eq. (1), r_0 can be expressed by Matsuoka et al. [9]

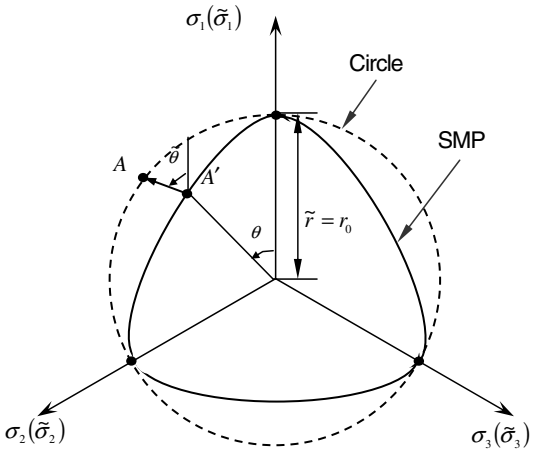

Fig. 1. SMP criterion in π-plane (solid curve) and transformed π-plane (broken circle).

$$\tilde{r} = r_0 = \sqrt{\frac{2}{3}} q^* = \sqrt{\frac{2}{3}} \frac{2I_1}{3\sqrt{(I_1 I_2 - I_3)/(I_1 I_2 - 9I_3)} - 1} \tag{2}$$

The generalized deviatoric stress in the transformed stress space $\tilde{q}(= \sqrt{3/2}\tilde{r})$ can be written as

$$\tilde{q} = q^* = \frac{2I_1}{3\sqrt{(I_1 I_2 - I_3)/(I_1 I_2 - 9I_3)} - 1} \tag{3}$$

To realize the transformation from σ_{ij} to $\tilde{\sigma}_{ij}$, the following equations should be made:

$$\begin{cases} \tilde{p} = p \\ \tilde{q} = q^* \\ \tilde{\theta} = f_1(\theta) \end{cases} \tag{4}$$

where $\tilde{p}$ is the mean transformed stress; $\tilde{\theta}$ and θ are Lode's stress angles in the transformed stress space and the ordinary stress space respectively, which are one-to-one correspondence with intermediate principal stress parameters $\tilde{b}$ and $b\,(=(\sigma_2 - \sigma_3)/(\sigma_1 - \sigma_3))$ in the transformed stress space and the ordinary stress space respectively; $f_1(\theta)$ is a function of θ which also can be expressed by b. So, Eq. (4) can be rewritten as

$$\begin{cases} \tilde{p} = p \\ \tilde{q} = q^* \\ \tilde{b} = f_2(b) \end{cases} \tag{5}$$

where

$$\begin{cases} \tilde{b} = \frac{\tilde{\sigma}_2 - \tilde{\sigma}_3}{\tilde{\sigma}_1 - \tilde{\sigma}_3} \\ \tilde{p} = \frac{1}{3}(\tilde{\sigma}_1 + \tilde{\sigma}_2 + \tilde{\sigma}_3) = \frac{1}{3}\tilde{\sigma}_{ii} \\ \tilde{q} = \frac{1}{\sqrt{2}}\sqrt{(\tilde{\sigma}_1 - \tilde{\sigma}_2)^2 + (\tilde{\sigma}_2 - \tilde{\sigma}_3)^2 + (\tilde{\sigma}_3 - \tilde{\sigma}_1)^2} \\ \quad = \sqrt{\frac{3}{2}(\tilde{\sigma}_{ij} - \tilde{p}\delta_{ij})(\tilde{\sigma}_{ij} - \tilde{p}\delta_{ij})} \end{cases} \tag{6}$$

$f_1(\theta)$ or $f_2(b)$ is a function to transform the flow direction of the plastic strain increment in the ordinary stress space into the flow direction in the transformed stress space. By

$f_1(\theta)$ or $f_2(b)$, the deviation of the plastic strain increment direction from the stress direction in the ordinary π-plane can be taken into consideration, although the directions of stress and plastic strain increments in transformed π-plane are coincident.

A reasonable plastic potential surface for frictional materials should be between the curved-triangle shape ($I_1I_2/I_3 = \text{const}$) and the circular shape ($q/p = \text{const}$) in the π-plane. So, the flow direction of the plastic strain increment is also between the normal to the triangular shape of SMP criterion and that to the circular shape, as shown Fig. 1. The following $f_2(b)$ [24] has the above characteristics

$$f_2(b) = \frac{\sqrt{\sigma_1} + \sqrt{\sigma_3}}{\sqrt{\sigma_2} + \sqrt{\sigma_3}} b = \frac{\sqrt{\sigma_2} - \sqrt{\sigma_3}}{\sqrt{\sigma_1} - \sqrt{\sigma_3}} \tag{7}$$

So, the transformed stress tensors under the general stress state can be obtained as

$$\tilde{\sigma}_{ij} = p\delta_{ij} + \frac{q^*}{q^s}(\sigma^s_{ij} - p^s\delta_{ij}) \tag{8}$$

and

$$\left.\begin{aligned} p^s &= \sigma^s_{ii}/3 \\ q^s &= \sqrt{(3/2)(\sigma^s_{ij} - p^s\delta_{ij})(\sigma^s_{ij} - p^s\delta_{ij})} \\ \sigma^s_{ij} &= (I^s_1\sigma_{ik} + I^s_3\delta_{ik})(\sigma_{kj} + I^s_3\delta_{kj})^{-1} \\ I^s_1 &= \sqrt{\sigma_1} + \sqrt{\sigma_2} + \sqrt{\sigma_3} \\ I^s_2 &= \sqrt{\sigma_1\sigma_2} + \sqrt{\sigma_2\sigma_3} + \sqrt{\sigma_3\sigma_1} \\ I^s_3 &= \sqrt{\sigma_1\sigma_2\sigma_3} \end{aligned}\right\} \tag{9}$$

When the stress tensor σ_{ij} is given, the transformed stress tensor $\tilde{\sigma}_{ij}$ can be calculated from Eq. (8). From the above derivation, it can be shown that the shape of the SMP criterion becomes a cone with the axis being the space diagonal $\tilde{\sigma}_1 = \tilde{\sigma}_2 = \tilde{\sigma}_3$ in the transformed principal stress space. Its cross-section is a circle with the center being the origin O in the $\tilde{\pi}$-plane (see Fig. 1). Noting the similarity in the shapes of the Extended Mises criterion in the principal stress space and the SMP criterion in the transformed principal stress space, we can revise existing elastoplastic models such as the Cam-clay model by using the transformed stress tensor $\tilde{\sigma}_{ij}$ based on the SMP criterion.

3. Basic method for constructing a unified hardening parameter independent of stress path

Hardening of materials is due to the occurrence of plastic strain. Therefore, a parameter representing the degree of hardening must depend on the plastic strain. Hardening parameters are internal variables that are used to indicate the rate of plastic deformation, and should be a function of plastic volumetric strain and plastic shear strain. For a single yield surface model, the hardening parameter should have the following properties: (1) its increments should be the same from one point on a yield surface to different points on another yield surface, and (2) its increment should also be same from one point to another point along different stress paths. Here, the hardening parameter is different with the hardening modulus which obviously changes from point to point. However, the plastic strain is usually dependent on the stress path. For example, the plastic volumetric strain and plastic shear strain for sand are all dependent on stress path (the test results in the following section can confirm this characteristic). So, the plastic strain increments instead of the total plastic strains should be used to construct a unified hardening parameter for various kinds of soils. That is to say, the hardening parameter should be a function of the plastic volumetric strain increment $d\varepsilon^p_v$ and the plastic shear strain increment $d\varepsilon^p_d$. It is assumed that the plastic volumetric strain increment and plastic shear strain increment can be related through the stress-dilatancy equation $d\varepsilon^p_v/d\varepsilon^p_d = f_1(\eta)$. For example, the stress-dilatancy equation in the original Cam-clay model is $d\varepsilon^p_v/d\varepsilon^p_d = M - \eta$ (stress ratio $\eta = q/p$; M is the value of η at the critical state), so that $f_1(\eta) = M - \eta$. Therefore, we can choose either the plastic volumetric strain increment $d\varepsilon^p_v$ or the plastic shear strain increment $d\varepsilon^p_d$ as a basic parameter to construct the hardening parameter. However, plastic shear strain does not occur during isotropic compression, which means that it is impossible to describe hardening under isotropic compression by use of the plastic shear strain increment. Therefore, we have to choose the plastic volumetric strain increment $d\varepsilon^p_v$ to construct the hardening parameter. Realizing that the increment of the hardening parameter should be independent of the stress path, we assume there exists a stress function $R(\eta)$ such that the integral $\int \frac{d\varepsilon^p_v}{R(\eta)}$ is independent of stress path. Thus, this integral can be used as a general hardening parameter

$$H = \int \frac{d\varepsilon^p_v}{R(\eta)} \tag{10}$$

In the Cam-clay model, $R(\eta) = 1$. A suitable $R(\eta)$ for both clay and sand will be introduced in the next section.

4. A unified hardening parameter for both clay and sand

A basic method for constructing a unified hardening parameter independent of stress path has been introduced in the preceding section. We will now derive a new hardening parameter for both clay and sand in this section. The modified Cam-clay model is considered to be one of the best basic elastoplastic models for clay, which is better than the original one [19]. In the modified Cam-clay model, the yield and plastic potential functions are assumed to be of the same form as follows:

$$f = g = \ln\frac{p}{p_0} + \ln\left(1 + \frac{q^2}{M^2p^2}\right) - \int \frac{d\varepsilon^p_v}{c_p} = 0 \tag{11}$$

where p_0 is the initial mean stress, $d\varepsilon^p_v (= d\varepsilon^p_{ii})$ is the plastic volumetric strain increment and c_p is written as

$$c_p = \frac{\lambda - \kappa}{1 + e_0} \tag{12}$$

with λ being the compression index, κ being the swelling index, and e_0 the initial void ratio at $p = p_0$. It is reasonable that Eq. (11) is also chosen as the plastic potential function for dilatant sand, because this equation predicts that the plastic volumetric strain increment is positive before the characteristic state ($\eta = M$) [7] and negative after the characteristic state (see Fig. 2). To adopt an associated flow rule in new model, a yield function similar to Eq. (11) is also assumed for sand. However, the plastic volumetric strain cannot be used as the hardening parameter for sand because it is dependent on the stress path and does not increase monotonically with loading. In this paper, a new hardening parameter H is derived to describe the hardening behavior of clay and sand. The yield and plastic potential functions for sand are written as

$$f = g = \ln\frac{p}{p_0} + \ln\left(1 + \frac{q^2}{M^2p^2}\right) - H = 0 \tag{13}$$

Nova and Wood [14,15] have chosen a combination of the plastic volumetric strain and plastic deviator strain as a hardening parameter. In the present model, the hardening parameter is considered to be a combination of the stress tensor σ_{ij} and plastic strain increment tensor $d\varepsilon^p_{ij}$, i.e., a plastic work type of hardening parameter. Thus, the following hardening parameter is assumed by using the plastic strain invariants

$$H = \int dH = \int \left[c_1(\sigma_{ij})d\varepsilon^p_v + c_2(\sigma_{ij})d\varepsilon^p_d\right] \tag{14}$$

where $c_1(\sigma_{ij})$ and $c_2(\sigma_{ij})$ are the functions of the stress tensor, respectively, and $d\varepsilon^p_d\left(=\sqrt{2/3}\sqrt{(d\varepsilon^p_{ij} - d\varepsilon^p_v\delta_{ij}/3)(d\varepsilon^p_{ij} - d\varepsilon^p_v\delta_{ij}/3)}\right)$ is the plastic deviator strain increment. In the modified Cam-clay model, the following stress-dilatancy equation is adopted:

$$\frac{d\varepsilon^p_v}{d\varepsilon^p_d} = \frac{M^2 - \eta^2}{2\eta} \tag{15}$$

Substituting Eq. (15) into (14) gives

$$H = \int \left[c_1(\sigma_{ij})d\varepsilon^p_v + c_2(\sigma_{ij})\frac{2\eta}{M^2 - \eta^2}d\varepsilon^p_v\right] = \int c(\sigma_{ij})d\varepsilon^p_v \tag{16}$$

where $c(\sigma_{ij})$ is a function of the stress tensor. Note that $c(\sigma_{ij})$ in Eq. (16) is also equal to $1/R(\eta)$ in Eq. (10). Fig. 3 shows the constant mean stress path (path AB) and the isotropic compression stress path (path AC) along which the hardening parameter changes from H_0 to H. The process for finding the hardening parameter H is (1) to derive a general equation of H along path AB and (2) to determine an explicit equation of H along path AC.

4.1. Along the constant mean stress path AB

After substituting Eq. (16) into Eq. (13), the total differential form of the yield function is expressed as

$$\begin{aligned} df &= \frac{\partial f}{\partial p}dp + \frac{\partial f}{\partial q}dq + \frac{\partial f}{\partial H}dH \\ &= \frac{\partial f}{\partial p}dp + \frac{\partial f}{\partial q}dq - c(\sigma_{ij})\Lambda\frac{\partial f}{\partial p} = 0 \end{aligned} \tag{17}$$

So the proportionality constant Λ can be written as

$$\Lambda = \frac{1}{c(\sigma_{ij})}\frac{\frac{\partial f}{\partial p}dp + \frac{\partial f}{\partial q}dq}{\frac{\partial f}{\partial p}} \tag{18}$$

Based on Eq. (13), the following two differential equations can be obtained:

$$\frac{\partial f}{\partial p} = \frac{1}{p}\frac{M^2 - \eta^2}{M^2 + \eta^2} \tag{19}$$

$$\frac{\partial f}{\partial q} = \frac{1}{p}\frac{2\eta}{M^2 + \eta^2} \tag{20}$$

By substituting Eqs. (19) and (20) into Eq. (18), the plastic deviator strain increment along a constant mean stress path is as follows:

$$d\varepsilon^p_d = \Lambda\frac{\partial f}{\partial q} = \frac{1}{c(\sigma_{ij})}\frac{1}{p}\frac{4\eta^2}{M^4 - \eta^4}dq \tag{21}$$

Fig. 4 shows the results of triaxial compression tests on clay and sand (data from [12]). It can be seen from Fig. 4a that the shapes of the curves $\eta \sim \varepsilon_d$ for clay and sand are alike. The stress ratios (q/p) at failure for clay and sand are M and M_f respectively. In fact, M_f is not constant during shearing. If the variation of M_f is considered during shearing, more complex behavior (e.g., the softening) of soils can be described [23]. In this paper, M_f is assumed to be constant for the sake of simplicity. The parameters M and M_f are similar to those of Nova and Wood [15].

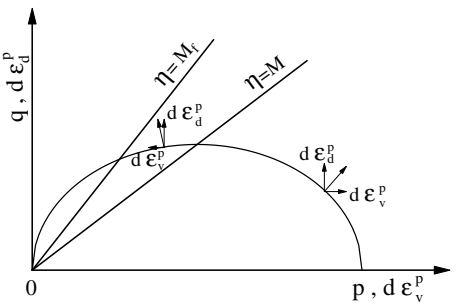

Fig. 2. Direction of plastic strain increment vectors.

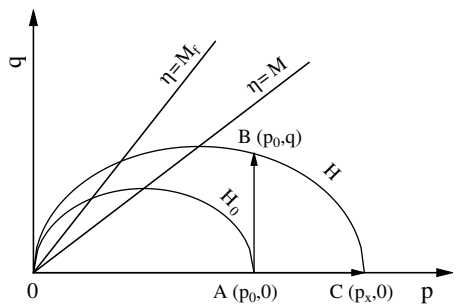

Fig. 3. Stress paths for deriving hardening parameter H.

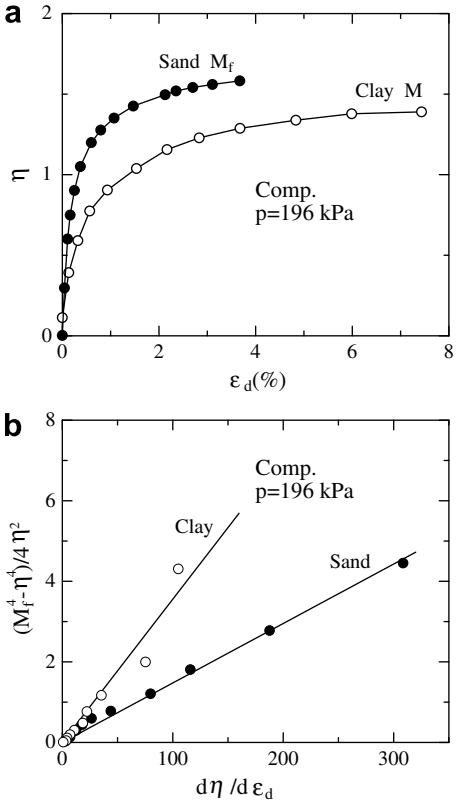

Fig. 4. Triaxial compression test results for clay and sand arranged in (a) $\eta \sim \varepsilon_d$; (b) $(M_f^4 - \eta^4)/4\eta^2 \sim d\eta/d\varepsilon_d$.

Therefore, compared with the equation of the plastic deviator strain increment for clay in the Cam-clay model when the mean stress is constant (Eq. (22)), the equation of the plastic deviator strain increment for sand is assumed to be Eq. (23) when the mean stress is constant

$$d\varepsilon_d^p = c_p \frac{1}{p} \frac{4\eta^2}{M^4 - \eta^4} dq \quad \text{(for clay)} \tag{22}$$

$$d\varepsilon_d^p = \rho \frac{1}{p} \frac{4\eta^2}{M_f^4 - \eta^4} dq \quad \text{(for sand)} \tag{23}$$

where ρ is a constant. Eqs. (22) and (23) can also be written in the linear forms

$$\frac{M^4 - \eta^4}{4\eta^2} = c_p \frac{d\eta}{d\varepsilon_d^p} \quad \text{(for clay)} \tag{24}$$

$$\frac{M_f^4 - \eta^4}{4\eta^2} = \rho \frac{d\eta}{d\varepsilon_d^p} \quad \text{(for sand)} \tag{25}$$

The validity of Eqs. (24) and (25) is confirmed by the triaxial compression results in Fig. 4b. So, the assumed form of Eq. (23) is appropriate. It is worth noting that $M_f = M$ for clay and the elastic deviator strain is very small under a constant mean stress in Fig. 4b. By combining Eqs. (21) and (23), $c(\sigma_{ij})$ in Eq. (21) is expressed as

$$c(\sigma_{ij}) = \frac{1}{\rho} \frac{M_f^4 - \eta^4}{M^4 - \eta^4} \tag{26}$$

Substituting Eq. (26) into Eq. (16) gives

$$H = \int dH = \int \frac{1}{\rho} \frac{M_f^4 - \eta^4}{M^4 - \eta^4} d\varepsilon_v^p \tag{27}$$

4.2. Along the isotropic compression stress path AC

When $\eta = 0$ (path AC), Eq. (27) becomes

$$H = \int dH = \int \frac{1}{\rho} \frac{M_f^4}{M^4} d\varepsilon_v^p \tag{28}$$

Moreover, under the isotropic compression condition ($\eta = q/p = 0$) and $\varepsilon_v^p = c_p \ln(p/p_0)$. In addition, Eq. (13) becomes $H = \ln(p/p_0)$ when $\eta = 0$. So, the following equation can be obtained from the above two equations:

$$H = \int dH = \int \frac{d\varepsilon_v^p}{c_p} \tag{29}$$

Letting Eq. (28) equal Eq. (29) gives

$$\rho = c_p \frac{M_f^4}{M^4} \tag{30}$$

Finally, we can obtain the following equation of the new hardening parameter for sand by substituting Eq. (30) into Eq. (27):

$$H = \int dH = \int \frac{1}{c_p} \frac{M^4}{M_f^4} \frac{M_f^4 - \eta^4}{M^4 - \eta^4} d\varepsilon_v^p \tag{31}$$

Comparing Eq. (10) with Eq. (31) gives

$$R(\eta) = c_p \frac{M_f^4}{M^4} \frac{M^4 - \eta^4}{M_f^4 - \eta^4} \tag{32}$$

If $M = M_f$, Eq. (31) becomes $H = \int dH = \int d\varepsilon_v^p / c_p$, which is the same as the hardening parameter for clay in the Cam-clay model. H in Eq. (31) is a unified one for both clay and sand.

5. A unified elastoplastic model for both clay and sand

In the proposed model, the equations of the yield locus and plastic potential remain the same as in Cam-clay, but the transformed stress tensor $\tilde{\sigma}_{ij}$ (based on the SMP criterion) and the new hardening parameter are adopted to model the mechanical behavior of clay and sand under three-dimensional stresses.

The total strain increment is given by the summation of the elastic component and the plastic component as usual:

$$d\varepsilon_{ij} = d\varepsilon_{ij}^e + d\varepsilon_{ij}^p \tag{33}$$

Here, the elastic component is given by the following equation

$$d\varepsilon_{ij}^e = \frac{1+v}{E} d\sigma_{ij} - \frac{v}{E} d\sigma_{mm} \delta_{ij} \tag{34}$$

where v is Poisson's ratio, and the elastic modulus E is expressed as

$$E = \frac{3(1-2v)(1+e_0)}{\kappa} p \tag{35}$$

The plastic component is given by assuming the flow rule not in σ_{ij} space but in $\tilde{\sigma}_{ij}$ space.

$$\mathrm{d}\varepsilon_{ij}^{\mathrm{p}} = \Lambda \frac{\partial g}{\partial \tilde{\sigma}_{ij}} \tag{36}$$

where the plastic potential function g (or the yield function f), the hardening parameter H, the proportionality constant Λ and the differential equation $\partial g/\partial \tilde{\sigma}_{ij}$ are given, respectively, as follows:

$$f = g = \ln \frac{\tilde{p}}{\tilde{p}_0} + \ln\left(1 + \frac{\tilde{q}^2}{M^2\tilde{p}^2}\right) - H = 0 \tag{37}$$

$$H = \int \mathrm{d}H = \int \frac{1}{c_p} \frac{M^4}{M_{\mathrm{f}}^4} \frac{M_{\mathrm{f}}^4 - \tilde{\eta}^4}{M^4 - \tilde{\eta}^4} \mathrm{d}\varepsilon_{\mathrm{v}}^{\mathrm{p}} \tag{38}$$

$$\Lambda = c_p \frac{M_{\mathrm{f}}^4}{M^4} \frac{M^4 - \tilde{\eta}^4}{M_{\mathrm{f}}^4 - \tilde{\eta}^4} \left(\mathrm{d}\tilde{p} + \frac{2\tilde{p}\tilde{q}}{M^2\tilde{p}^2 - \tilde{q}^2} \mathrm{d}\tilde{q}\right) \tag{39}$$

$$\frac{\partial g}{\partial \tilde{\sigma}_{ij}} = \frac{1}{M^2\tilde{p}^2 + \tilde{q}^2} \left[\frac{M^2\tilde{p}^2 - \tilde{q}^2}{3\tilde{p}} \delta_{ij} + 3(\tilde{\sigma}_{ij} - \tilde{p}\delta_{ij})\right] \tag{40}$$

In the above equations, the deviator stress $\tilde{q}$ and the transformed stress ratio $\tilde{\eta}$ in $\tilde{\sigma}_{ij}$ space, $M(\tilde{\eta}$ at critical state) and $M_{\mathrm{f}}(\tilde{\eta}$ at peak) are written respectively as follows:

$$\tilde{\eta} = \tilde{q}/\tilde{p} \tag{41}$$

$$\tilde{q} = \sqrt{\frac{3}{2}\tilde{s}_{ij}\tilde{s}_{ij}} \tag{42}$$

$$M = \frac{6\sin\phi_{\mathrm{c}}}{3 - \sin\phi_{\mathrm{c}}} \tag{43}$$

$$M_{\mathrm{f}} = \frac{6\sin\phi}{3 - \sin\phi} \tag{44}$$

where $\tilde{p}_0 (= p_0)$ is the initial mean stress, and $(\phi_{\mathrm{c}}, \phi)$ are the internal friction angles at the characteristic state and shear failure, respectively. The main features of the proposed model for both clay and sand are presented as follows.

5.1. For sand

The stress-dilatancy equation of the proposed model is expressed as follows:

$$\frac{\mathrm{d}\varepsilon_{\mathrm{v}}^{\mathrm{p}}}{\mathrm{d}\varepsilon_{\mathrm{d}}^{\mathrm{p}}} = \frac{M^2\tilde{p}^2 - \tilde{q}^2}{2\tilde{p}\tilde{q}} \tag{45}$$

Eq. (45) can be drawn as Fig. 5a in the $\tilde{q}/\tilde{p} \sim -\mathrm{d}\varepsilon_{\mathrm{v}}^{\mathrm{p}}/\mathrm{d}\varepsilon_{\mathrm{d}}^{\mathrm{p}}$ plane and as Fig. 5b in the $q/p \sim -\mathrm{d}\varepsilon_{\mathrm{v}}^{\mathrm{p}}/\mathrm{d}\varepsilon_{\mathrm{d}}^{\mathrm{p}}$ plane under triaxial compression and extension conditions. It is seen from these two figures that the unique relationship between $\tilde{q}/\tilde{p}$ and $-\mathrm{d}\varepsilon_{\mathrm{v}}^{\mathrm{p}}/\mathrm{d}\varepsilon_{\mathrm{d}}^{\mathrm{p}}$ can explain the difference in the $q/p \sim -\mathrm{d}\varepsilon_{\mathrm{v}}^{\mathrm{p}}/\mathrm{d}\varepsilon_{\mathrm{d}}^{\mathrm{p}}$ relations between triaxial compression and extension.

Under triaxial compression and extension stress conditions, the yield function in Eq. (37) is plotted in Fig. 6, where CL and FL show the characteristic state line and the shear failure line, respectively. $\tilde{\sigma}_{\mathrm{a}}$ and $\tilde{\sigma}_{\mathrm{r}}$ are the transformed stresses corresponding to σ_{a} and σ_{r} respectively, in which σ_{a} and σ_{r} are the axial and radial stresses in triaxial stress conditions. It is seen from Fig. 6 that although the yield curves in triaxial compression and extension are symmetrical with respect to the $\tilde{p}$-axis in the $\tilde{p} \sim (\tilde{\sigma}_{\mathrm{a}} - \tilde{\sigma}_{\mathrm{r}})$ plane (see Fig. 6a), the yield curves are not symmetrical with respect to p-axis, and the value of q in triaxial extension is smaller than that in triaxial compression in the $p \sim (\sigma_{\mathrm{a}} - \sigma_{\mathrm{r}})$ plane at the same p (see Fig. 6b). This trend is similar to the test results from various kinds of soils (e.g., [10]).

How the proposed model describes the dilatancy of soil is explained as follows. From Eq. (38), we obtain

$$\mathrm{d}\varepsilon_{\mathrm{v}}^{\mathrm{p}} = c_p \frac{M_{\mathrm{f}}^4}{M^4} \frac{M^4 - \tilde{\eta}^4}{M_{\mathrm{f}}^4 - \tilde{\eta}^4} \mathrm{d}H \tag{46}$$

Since $\mathrm{d}H$ is always larger than or equal to 0, the following conclusions can be obtained from Eq. (46):

(1) $\tilde{\eta} = 0$ (isotropic compression condition): $\mathrm{d}\varepsilon_{\mathrm{v}}^{\mathrm{p}} = c_p \mathrm{d}H$.
(2) $0 \leqslant \tilde{\eta} < M$ (negative dilatancy condition): $\mathrm{d}\varepsilon_{\mathrm{v}}^{\mathrm{p}} > 0$.
(3) $\tilde{\eta} = M$ (characteristic state condition): $\mathrm{d}\varepsilon_{\mathrm{v}}^{\mathrm{p}} = 0$.
(4) $M < \tilde{\eta} \leqslant M_{\mathrm{f}}$ (positive dilatancy condition): $\mathrm{d}\varepsilon_{\mathrm{v}}^{\mathrm{p}} < 0$.

As indicated above, the dilatancy of clay and sand are reasonably described by the new hardening parameter H. The validity of H and the other quantities used usually as hardening parameters will be checked in the various stress paths as follows.

Fig. 7 shows the stress paths in triaxial tests on Toyoura sand (data from [11]) in terms of the relation between mean stress p and deviator stress q. The values of the principal stress ratios are the same ($\sigma_1/\sigma_3 = 4$) at points F and F' in Fig. 7. We will check the stress path dependency of four quantities, the plastic volumetric strain $\varepsilon_{\mathrm{v}}^{\mathrm{p}}$, the plastic deviator strain $\varepsilon_{\mathrm{d}}^{\mathrm{p}}$, the plastic work W^{p} and the proposed hardening parameter H, in four kinds of triaxial compression tests (paths: ADEF, ABCF, AGF and ABEF) and three kinds of triaxial extension tests (paths: AD′F′, ACF′ and AF′).

Figs. 8–11 show the variations of those quantities along the seven kinds of stress paths under triaxial compression and extension conditions. It is obvious from Figs. 8 and 9 that the plastic volumetric strain $\varepsilon_{\mathrm{v}}^{\mathrm{p}}$ and the plastic deviator strain $\varepsilon_{\mathrm{d}}^{\mathrm{p}}$ are unsuitable for the hardening parameter for sand because these quantities depend on the stress paths at the same stress state. From Fig. 10 the plastic work W^{p} is almost independent of the stress paths only in triaxial compression or triaxial extension, but its value at the stress state F is different from that at F' although the stress invariants ($\tilde{p}$ and $\tilde{q}$) of the stress states F and F' are the same. The other problem induced by the plastic work hardening parameter is that sand will always harden even though it is at a peak or failure state. Hence, the plastic work is also not good for the hardening parameter in general stress states. However, Fig. 11 shows that the values of the

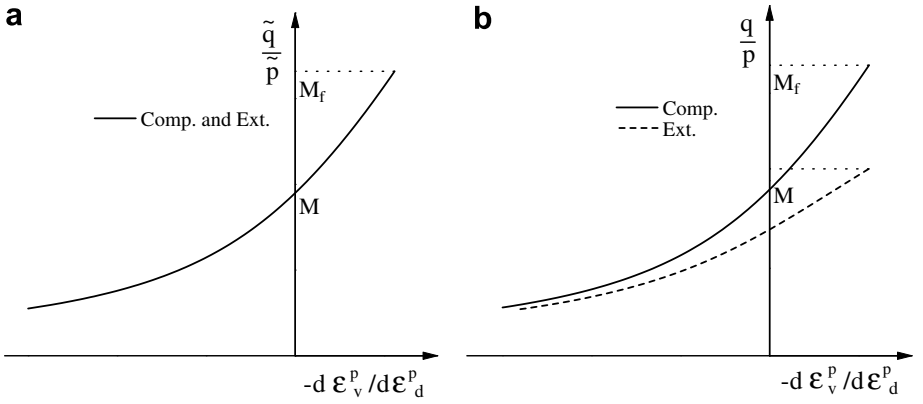

Fig. 5. Stress-dilatancy relationships of proposed model under triaxial compression and extension conditions expressed in (a) $\tilde{q}/\tilde{p} \sim -\mathrm{d}\varepsilon_v^p/\mathrm{d}\varepsilon_d^p$ and (b) $q/p \sim -\mathrm{d}\varepsilon_v^p/\mathrm{d}\varepsilon_d^p$.

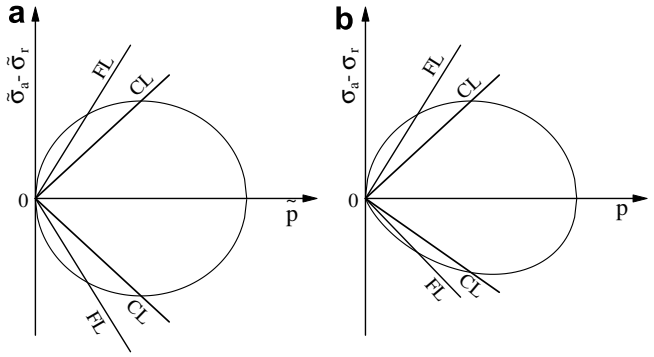

Fig. 6. Yield curves of proposed model under triaxial compression and extension conditions expressed in (a) $\tilde{p} \sim (\tilde{\sigma}_a - \tilde{\sigma}_r)$ plane and (b) $p \sim (\sigma_a - \sigma_r)$ plane.

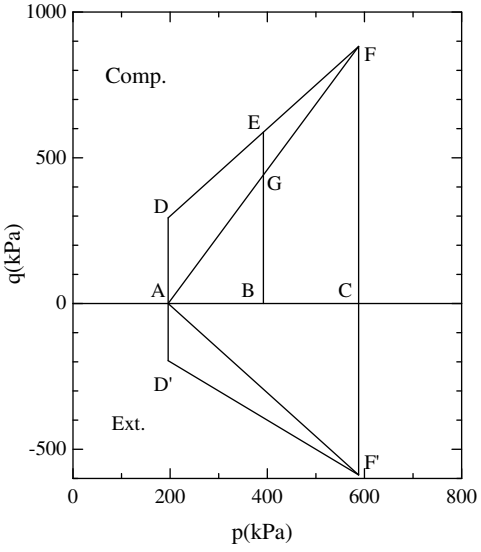

Fig. 7. Stress paths of triaxial tests for examining new hardening parameter.

proposed hardening parameter H are uniquely determined at the same stress state, regardless of the stress path in triaxial compression and extension and the previous stress

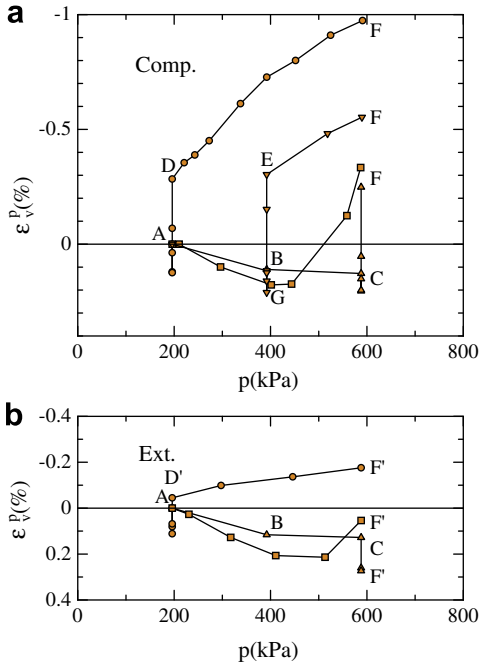

Fig. 8. Relation between plastic volumetric strain ε_v^p and mean principal stress p.

history. So, the proposed hardening parameter H is a state quantity, and we employ it as a new hardening parameter for sand.

5.2. For clay

As mentioned before, if $M = M_f$, the new hardening parameter H becomes the plastic volumetric strain, which is the same as the hardening parameter for normally consolidated clay in the Cam-clay model. Therefore, in this case the difference between the proposed model and the Cam-clay model is only the stress tensor used. Let us discuss the critical state conditions in three-dimensional stresses in detail. The critical state conditions of the proposed model in three-dimensional stresses can be expressed as follows:

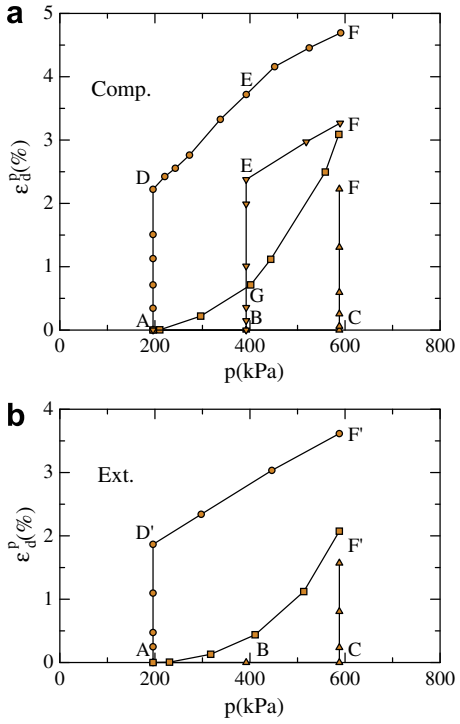

Fig. 9. Relation between plastic deviator strain ε_d^p and mean principal stress p.

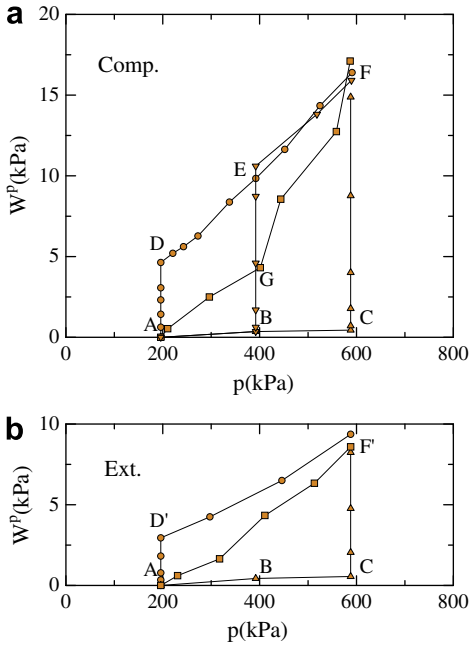

Fig. 10. Relation between plastic work W^p and mean principal stress p.

$$\left.\begin{aligned}&\tilde{\eta}_{cs} = \tilde{q}_{cs}/\tilde{p}_{cs} = M\\ &d\varepsilon_v^p/d\varepsilon_d^p = 0\\ &\varepsilon_v^p = c_p[\ln(\tilde{p}_{cs}/\tilde{p}_0) + \ln 2]\\ &\varepsilon_d^p \to \infty\end{aligned}\right\} \tag{47}$$

where the suffix cs means the critical state. When Eq. (47) is satisfied, soil will be continuously distorted. Eq. (47) is the same as the critical state conditions of the Cam-clay model in triaxial compression, so we might say Eq. (47) is the extension form for the critical state conditions of the Cam-clay model under three-dimensional stresses.

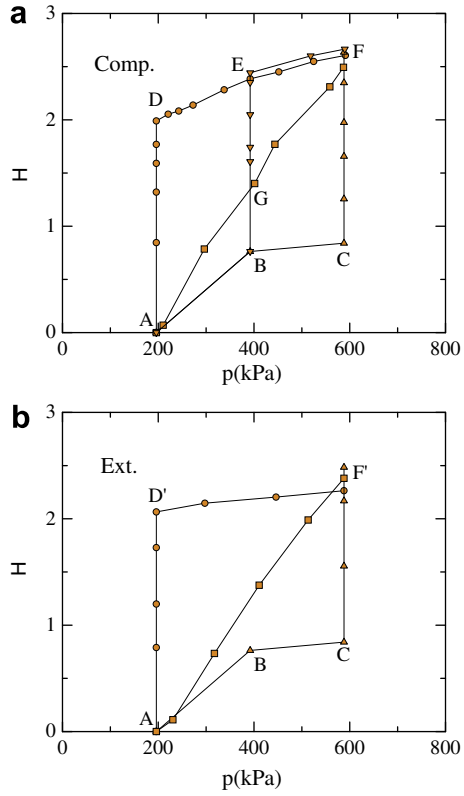

Fig. 11. Relation between new hardening parameter H and mean principal stress p.

6. Predictions versus experimental results

A series of triaxial compression and triaxial extension tests on normally consolidated Fujinomori clay and saturated Toyoura sand have been completed by Nakai and Matsuoka [12] and Nakai [11]. Fig. 12 shows the initial yield surfaces from Eq. (37) and the test stress paths conducted in triaxial compression and extension for clay and sand. The test data are used to examine the capability of the proposed model in predicting drained behavior of clay and sand. The values of soil parameters used in the model are $M = M_f = 1.45$, $\lambda/(1+e_0) = 0.0508$, $\kappa/(1+e_0) = 0.0112$ and $\nu = 0.3$ for Fujinomori clay, and $M = 0.95$, $M_f = 1.66$, $\lambda/(1+e_0) = 0.00403$, $\kappa/(1+e_0) = 0.00251$ and $\nu = 0.3$ for Toyoura sand, respectively. The above soil parameters are determined from isotropic compression tests and conventional triaxial compression tests.

6.1. Path p = const

Fig. 13 compares the predicted and observed results for the drained behavior of Fujinomori clay and Toyoura sand under triaxial compression and extension conditions when

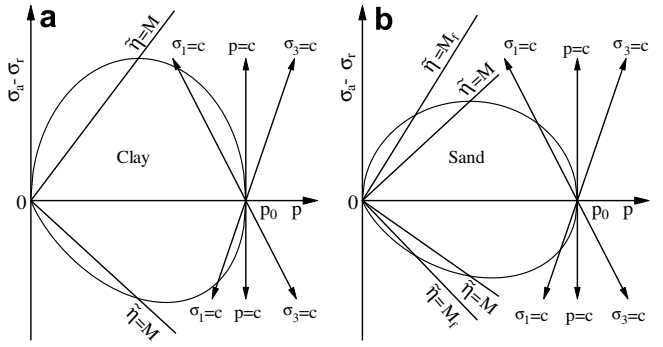

Fig. 12. Stress paths in triaxial compression and extension tests for (a) clay and (b) sand.

$p = 196$ kPa. It can be seen from this figure that the predictions (solid lines) of the proposed model agree well with the observed test results (marked ○) for clay and sand at constant mean stress under triaxial compression and extension conditions.

6.2. Path σ_3 = const

Fig. 14 compares the predicted and observed test results for the drained behavior of Fujinomori clay and Toyoura sand under triaxial compression and extension conditions when $\sigma_3 = 196$ kPa. It can be seen from this figure that the predictions (solid lines) of the proposed model agree well with the observed test results (marked ○) for clay

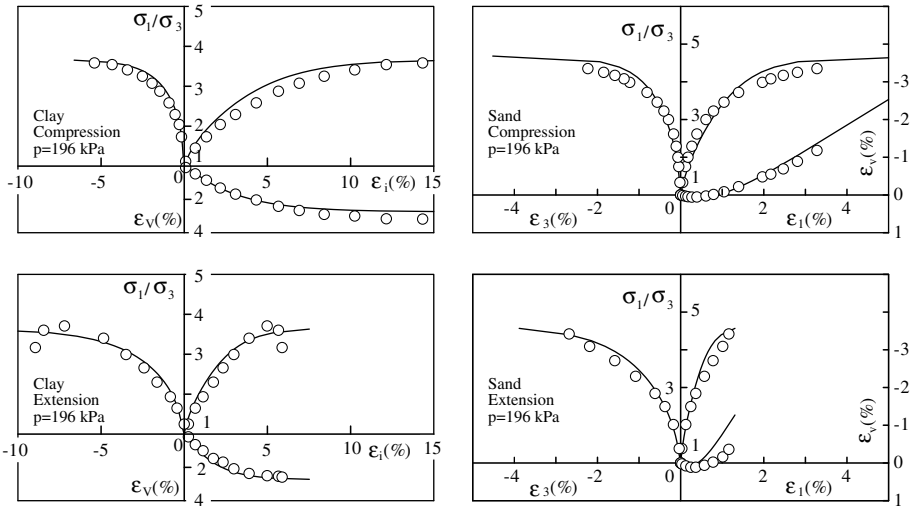

(a) For clay (b) For sand

Fig. 13. Comparison between predicted and test results under triaxial compression and extension conditions when p = constant for clay and sand.

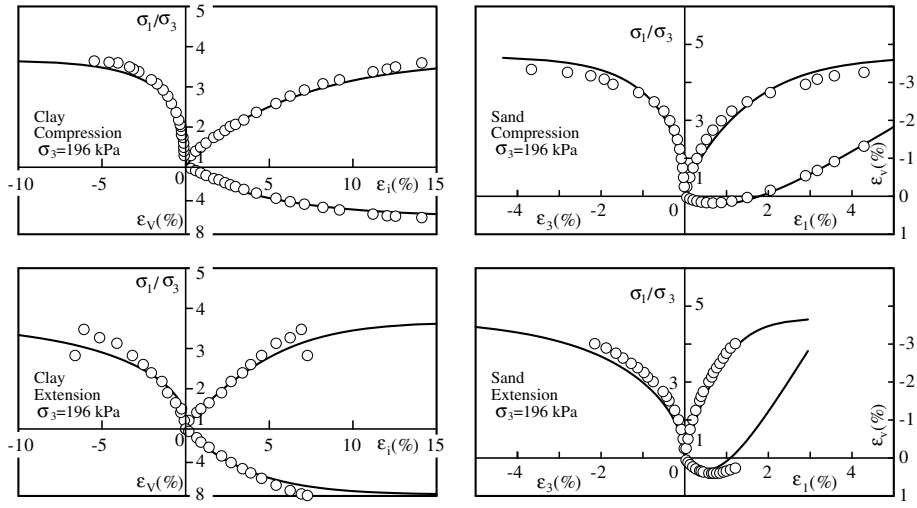

(a) For clay (b) For sand

Fig. 14. Comparison between predicted and test results under triaxial compression and extension conditions when σ_3 = constant for clay and sand.

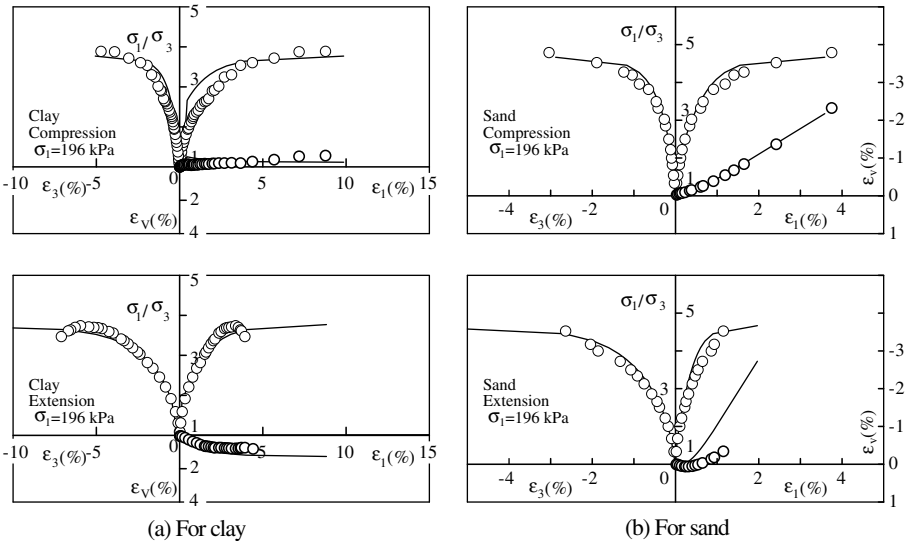

Fig. 15. Comparison between predicted and test results under triaxial compression and extension conditions when $\sigma_1 =$ constant for clay and sand.

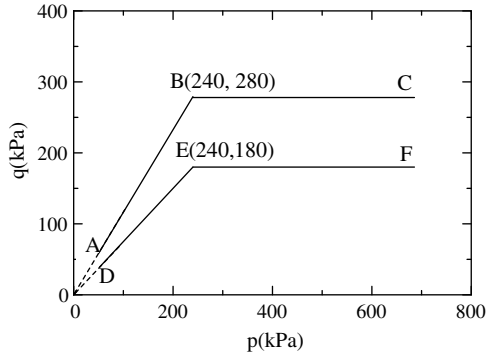

Fig. 16. Stress paths including constant and decrease in stress ratio in triaxial compression for sand.

and sand with increasing mean stress under triaxial compression and extension conditions.

6.3. Path σ_1 = const

Fig. 15 compares the predicted and observed test results for the drained behavior of Fujinomori clay and Toyoura sand under triaxial compression and extension conditions when $\sigma_1 = 196$ kPa. Since the most of the stress path in triaxial compression for clay is within the initial yield surface (Fig. 12a), the predicted strain is a little smaller than the

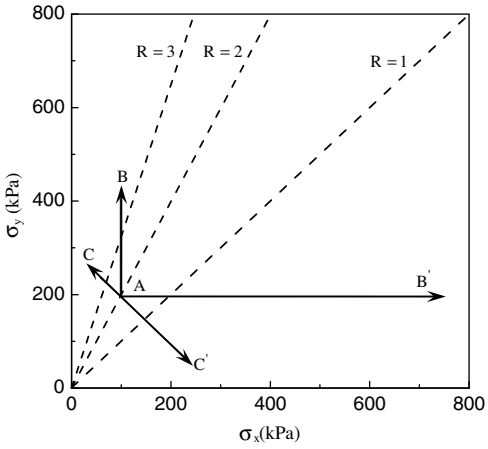

Fig. 18. Stress paths under plane strain condition.

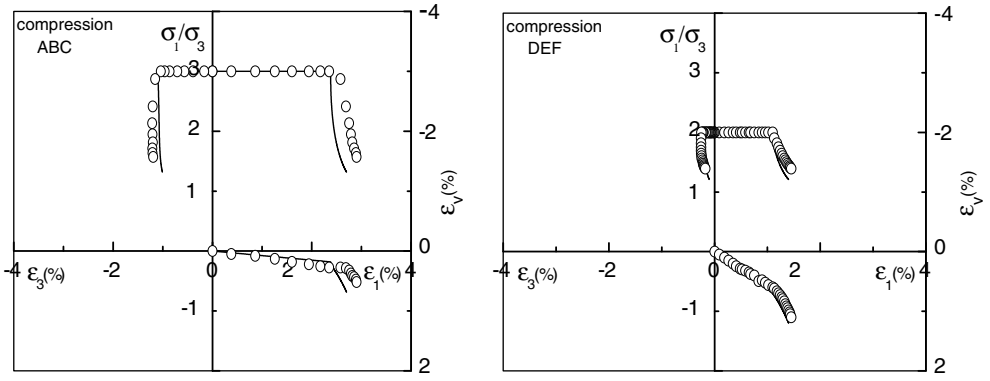

Fig. 17. Comparison between predicted and test results along stress paths ABC and DEF in triaxial compression for sand.

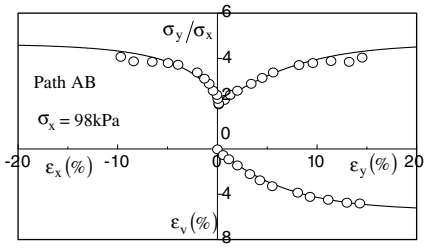

(a) Stress-strain behavior

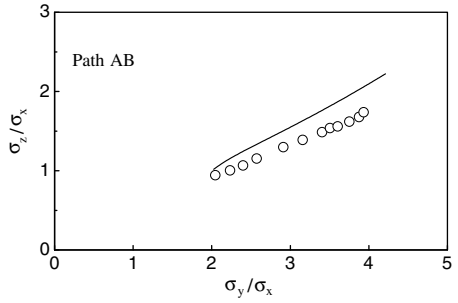

(b) Intermediate principal stress

Fig. 19. Comparison between predicted and measured (a) stress–strain behavior and (b) intermediate principal stress under plane strain path AB without change in principal stress directions (data after [13]).

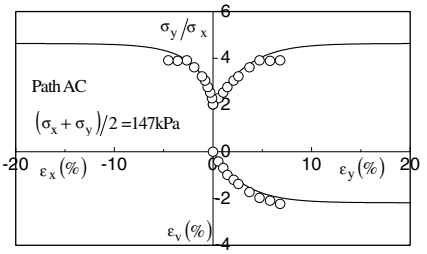

(a) Stress-strain behavior

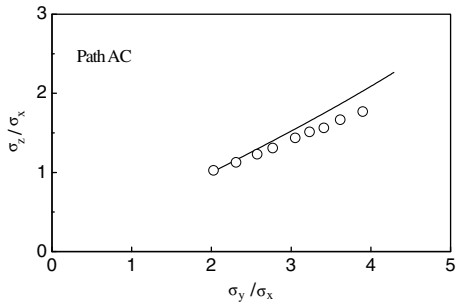

(b) Intermediate principal stress

Fig. 20. Comparison between predicted and measured (a) stress–strain behavior and (b) intermediate principal stress under plane strain path AC without change in principal stress directions (data after [13]).

test results (Fig. 15a). But, it can be seen from Fig. 15a and b that the predicted results (solid lines) agree well with the test results (marked ○) for clay under triaxial extension condition and for sand under triaxial compression and extension conditions.

6.4. Stress paths including constant and decrease in stress ratio in triaxial compression for sand

Fig. 16 shows two special stress paths, which contain a constant and a decrease in stress ratio under triaxial compression, for tests on a sand. The values of the sand parameters used in the model are $M = 1.08$, $M_f = 1.68$, $\lambda/(1 + e_0) = 0.00462$, $\kappa/(1 + e_0) = 0.00259$ and $v = 0.3$, respectively. The above soil parameters were determined by an isotropic compression test and a conventional triaxial compression test.

Fig. 17 shows the predicted and observed test results for the drained stress–strain behavior along the stress paths ABC and DEF, respectively. It can be seen from this figure that the results (solid lines) predicted by the proposed model agree well with the test results (marked ○) in those special stress paths.

6.5. Stress paths in plane strain for clay

In order to validate the present model under plane strain condition, the model is used to predict the results of the plane strain tests on Fujinomori clay [13].

Fig. 18 shows the stress paths tested in the plane strain tests. The tests are conducted along four kinds of stress paths (AB, AC, AB′ and AC′) under plane strain condition from K_0-consolidation state (point A: $\sigma_y = 196$ kPa, $\sigma_x = \sigma_z = 98$ kPa). The model parameters used in the predictions are the same as the above for Fujinomori clay.

Figs. 19 and 20 show the comparison between predicted and measured stress–strain behavior and intermediate principal stress along paths AB and path AC, respectively, without change in principal stress directions.

Figs. 21 and 22 show the comparison between predicted and measured stress–strain behavior and intermediate prin-

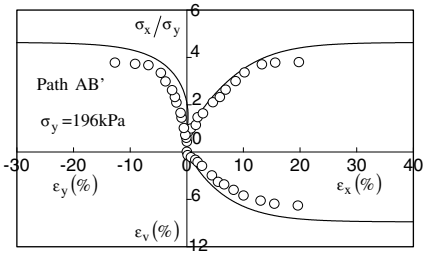

(a) Stress-strain behavior

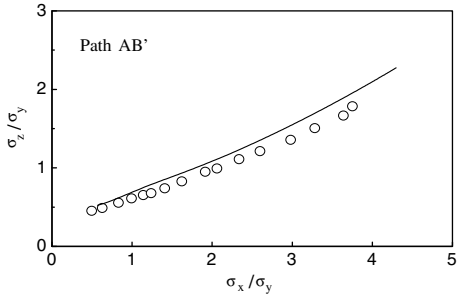

(b) Intermediate principal stress

Fig. 21. Comparison between predicted and measured (a) stress–strain behavior and (b) intermediate principal stress under plane strain path AB′ with change in principal stress directions (data after [13]).

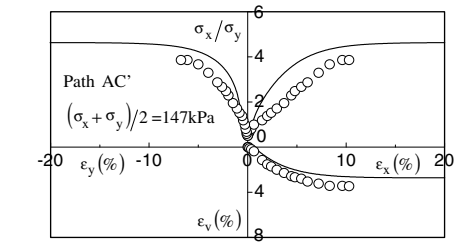

(a) Stress-strain behavior

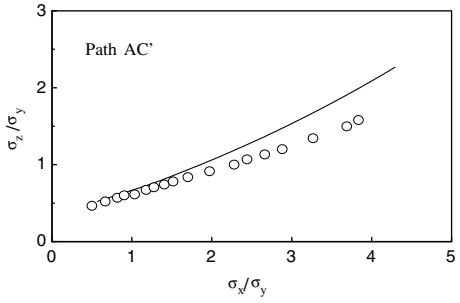

(b) Intermediate principal stress

Fig. 22. Comparison between predicted and measured (a) stress–strain behavior and (b) intermediate principal stress under plane strain path AC′ with change in principal stress directions (data after [13]).

cipal stress along paths AB′ and path AC′, respectively, with change in principal stress directions.

It is seen from Figs. 19–22 that the present model gives relatively good predictions of the measured stress–strain behavior and the measured intermediate principal stress values.

Therefore, it can be seen from the above comparisons that the proposed model can reasonably describe the stress–strain characteristics of clay and sand under three-dimensional stresses, as well as the dilatancy of sand along various stress paths.

7. Conclusions

(1) A new hardening parameter is derived by considering unified yield and plastic potential functions for both clay and sand. It not only describes the dilatancy for lightly to heavily dilatant sand, but also reduces to the plastic volumetric strain for clay. The validity of the hardening parameter is confirmed by triaxial compression and extension tests on sand along various stress paths.

(2) An elastoplastic model is proposed by applying the transformed stress tensor $\tilde{\sigma}_{ij}$ (based on the SMP criterion) and the new hardening parameter H to the Cam-clay model. The proposed model can reasonably describe the stress–strain behavior of clay and sand under three-dimensional stress states.

(3) The five soil parameters (λ, κ, M, M_f and ν) in the proposed model can be determined by a loading and unloading isotropic compression test and a conventional triaxial compression test.

Acknowledgements

This study was supported by the National Natural Science Foundation of China, NSFC (No. 10672010 and No. 50479001). The authors thank Prof. S.W. Sloan and Dr. D.C. Sheng at the University of Newcastle, Australia, for their helps in improving the quality of the paper. The authors are also appreciative of the contributions made by D.C. Lu and W. Hou at Beihang University, China, who made part of the predictions in this paper.

References

[1] Anandarajah A. A granular material model based on associated flow rule applied to monotonic loading behavior. Soils Found 1994;34(3):81–98.
[2] Bardet JP. A bounding surface model for sands. ASCE J Eng Mech 1986;112(EM11):1198–217.
[3] Dafalias YF. Bounding surface plasticity. I: Theory. ASCE J Eng Mech 1986;112(EM12):1242–91.
[4] Hashiguchi K, Ueno M. Elasto-plastic constitutive laws of glandular materials. In: Proceedings of special session 9 of 9th international conference on soil mechanics and foundations engineering, Tokyo, 1977. p. 73–82.
[5] Lade PV. Elasto-plastic stress–strain theory for cohesionless soils with curved yield surface. Int J Solids Struct 1977;13:1019–35.
[6] Lade PV, Prabucki MJ. Softening and preshearing effects in sand. Soils Found 1995;35(4):95–104.
[7] Luong MP. Stress–strain aspects of cohesionless soils under cyclic and transient loading. In: International symposium on soils under cyclic and transient loading, 1982. p. 315–24.
[8] Matsuoka H, Nakai T. Stress-deformation and strength characteristics of soil under three difference principal stresses. Proc JSCE 1974;232:59–70.
[9] Matsuoka H, Yao YP, Sun DA. The Cam-clay models revised by the SMP criterion. Soils Found 1999;39(1):79–99.
[10] Miura N, Murata H, Yasufuku N. Stress strain characteristics of sand in a particle-crushing region. Soils Found 1984;24(1):77–89.
[11] Nakai T. An isotropic hardening elastoplastic model for sand considering the stress path dependency in three-dimensional stresses. Soils Found 1989;29(1):119–37.
[12] Nakai T, Matsuoka H. A generalized elastoplastic constitutive model for clay in three-dimensional stresses. Soils Found 1986;26(3):81–98.
[13] Nakai T, Tsuzuki K, Yamamoto M, Hishida T. Analysis of plane strain tests on normally consolidated clay by an elastoplastic constitutive model. In: Proceedings of the 21st Japan national conference on soil mechanics and foundation engineering, vol. 2, 1986. p. 453–56 [in Japanese].
[14] Nova R, Wood DM. An experimental programme to define the yield function for sand. Soils Found 1978;18(4):77–86.
[15] Nova R, Wood DM. A constitutive model for sand in triaxial compression. Int J Numer Anal Methods Geomech 1979;3:255–78.
[16] Pastor M, Zienkiewicz OC, Leung KH. A simple model for transient loading in earthquake analysis. Part II: Non-associative model for sands. Int J Numer Anal Methods Geomech 1985;9:477–98.
[17] Prevost JH. A simple plasticity theory for frictional cohesionless soils. Soil Dyn Earthquake Eng 1985;4(1):9–17.
[18] Roscoe KH, Burland JB. On the generalised stress–strain behavior of 'wet' clay. In: Heyman J, Leckie FA, editors. Engineering plasticity. Cambridge, England: Cambridge University Press; 1968. p. 535–609.
[19] Roscoe KH, Schofield AN, Thurairajah A. Yielding of clay in states wetter than critical. Geotechnique 1963;13:211–40.

[20] Sheng D, Sloan SW, Yu HS. Aspects of finite element implementation of critical state models. Comput Mech 2000;26(2):185–96.
[21] Sloan SW, Abbo AJ, Sheng D. Refined explicit integration of elastoplastic models with automatic error control. Eng Comput 2001;18(1–2):121–54.
[22] Wroth CP, Houlsby GT. Soil mechanics-property characterization and analysis procedures. In: Proceedings of 11th international conference on soil mechanics and foundations engineering, San Francisco, vol. 1, 1985. p. 1–55.
[23] Yao YP, Matsuoka H, Sun DA. A unified elastoplastic model of sand dependent on stress level and void ratio. In: Proceedings of 2nd international symposium on pre-failure deformation characteristics of geomaterials, September 27–29, Torino, Italy, 1999. p. 589–96.
[24] Yao YP, Sun DA. Application of Lade's criterion to Cam-clay model. J Eng Mech ASCE 2000;126(1):112–9.
[25] Yao YP, Sun DA. Application of Lade's criterion to Cam-clay model (Closure). J Eng Mech ASCE 2001;127(6):631–3.
[26] Yu HS. CASM: A unified state parameter model for clay and sand. Int J Numer Anal Methods Geomech 1998;22:621–53.
[27] Zienkiewicz OC, Leung KH, Pastor M. A simple model for transient loading in earthquake analysis. Part I: Basic model. Int J Numer Anal Methods Geomech 1985;9:453–76.